



## Joint coding-denoising optimization of noisy images

Mikael Carlavan, Laure Blanc-Féraud, Marc Antonini, Carole Thiebaud,  
Christophe Latry, Yves Bobichon

### ► To cite this version:

Mikael Carlavan, Laure Blanc-Féraud, Marc Antonini, Carole Thiebaud, Christophe Latry, et al..  
Joint coding-denoising optimization of noisy images. [Research Report] I3S. 2013. hal-00773604

**HAL Id: hal-00773604**

**<https://inria.hal.science/hal-00773604>**

Submitted on 14 Jan 2013

**HAL** is a multi-disciplinary open access archive for the deposit and dissemination of scientific research documents, whether they are published or not. The documents may come from teaching and research institutions in France or abroad, or from public or private research centers.

L'archive ouverte pluridisciplinaire **HAL**, est destinée au dépôt et à la diffusion de documents scientifiques de niveau recherche, publiés ou non, émanant des établissements d'enseignement et de recherche français ou étrangers, des laboratoires publics ou privés.

# Joint coding-denoising optimization of noisy images

Mikael Carlván, Laure Blanc-Féraud, Marc Antonini, Carole Thiebaut, Christophe Latry  
and Yves Bobichon

## Abstract

In this paper, we propose to study the problem of noisy source coding/denoising. The challenge of this problem is that a global optimization is usually difficult to perform as the global fidelity criterion needs to be optimized in the same time over the sets of both coding and denoising parameters. Most of the bibliography in this domain is based on the fact that, for a specific criterion, the global optimization problem can be simply separated into two independent optimization problems: The noisy image should be first optimally denoised and this denoised image should then be optimally coded. In many applications however, the layout of the acquisition imaging chain is fixed and cannot be changed, that is a denoising step cannot be inserted before coding. For this reason, we are concerned here with the problem of global joint optimization in the case the denoising step is performed, as usual, after coding/decoding. In this configuration, we show how to express the global distortion as a function of the coding and denoising parameters. We present then an algorithm to minimize this distortion and to get the optimal values of these parameters. We show results of this joint optimization algorithm on classical test images and on a high dynamic range image, visually and in a rate-distortion sense.

## Index Terms

Global optimization, noisy source coding, quantizing, image denoising

M. Carlván and L. Blanc-Féraud are with MORPHEME team, joint project between INRIA, CNRS and the University of Nice-Sophia Antipolis; M. Antonini is with I3S laboratory UMR7271 University of Nice Sophia-Antipolis and CNRS, 2000 route des Lucioles, Les Algorithmes - bât. Euclide B, 06903 Sophia Antipolis, France (e-mail: carlván@i3s.unice.fr, blancf@i3s.unice.fr, am@i3s.unice.fr).

C. Thiebaut and C. Latry are with CNES, 18 avenue Edouard Belin, 31401 Toulouse, France (e-mail: Carole.Thiebaut@cnes.fr, Christophe.Latry@cnes.fr).

Y. Bobichon is with Thales Alenia Space, 100 boulevard du Midi, 06156 Cannes la Bocca, France (e-mail: yves.bobichon@thalesaleniaspace.com).

## I. INTRODUCTION

Images acquired by imaging systems are most of the time degraded by noise, which mainly comes from the imperfections of optical instruments. It is well-known that noise decreases the performances of coding schemes as it reduces the correlation between pixels [1]. This problem is commonly referred as the noisy source coding problem [2]. Many works have been devoted to address this issue [3], [4], [5], [6], [7], [8] and [9]. The majority of the mentioned works are based on the study of the global distortion optimization initially proposed by [5] and refined in [6]. This study states that the global distortion, if measured by the Mean Square Error (MSE), can be treated as two separated problems. First, the original source image should be optimally, in the minimum MSE sense, estimated from the noisy data and this estimate should then be optimally coded [6].

However, adding a supplementary step before coding is not always possible and in many cases the noisy acquired images are directly encoded without pre-processing. Critical applications such as satellite imaging can not indeed afford to insert pre-processing steps in the acquisition imaging chain as the on-board resources are highly limited. But one is still interested in optimizing the global imaging chain to obtain the best final image. So the imaging chain has to be considered as it is and the global distortion of this chain needs to be optimized. This is the focus of this paper.

More precisely, we are considering here the problem of optimal joint coding/denoising of a noisy image and focus on the acquisition imaging chain depicted figure 1. We show that, under certain hypotheses that we will describe, a closed-form expression of the global distortion can be obtained. We propose then to optimize this distortion, with respect to the coding and the denoising parameters, to reach the minimum global distortion. The originality of the proposed approach relies on the fact that we propose a global joint optimization which takes into account all the parameters of the imaging chain. We will also show that treating the optimization of coding/denoising as two separate problems (as in [7], [8], [9]) is suboptimal when the denoising is performed after coding. More precisely, we emphasize the necessity to take into account the denoising step in the rate-distortion allocation of the coder. And, as we will see, this requirement is confirmed by the results which display a significant improvement in comparison to the classical method which executes coding and denoising separately.

The paper is organized as follows. In section II, we present the studied imaging chain and introduce

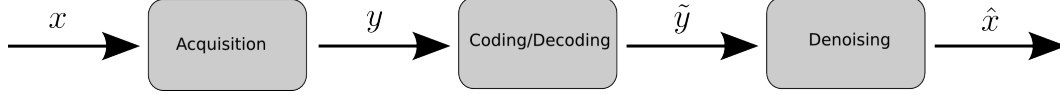


Fig. 1. Considered acquisition imaging chain.

hypotheses and notations. We detail in section III the proposed approach and we show how to get a closed-form expression of the global distortion for the studied case. We detail the joint optimization of this distortion in section IV and we present the algorithm to get the optimal parameters of the coding and the denoising steps. We show results, visually and in a rate-distortion sense, of the proposed joint optimization algorithm on classical test images and on a remote sensing image, in section V. We conclude in section VI and present perspectives for future works.

## II. HYPOTHESES AND NOTATIONS

In the following, the operators applied to the image are denoted with a bold uppercase letter. The non-bold uppercase letters represent random variables whose realizations are denoted by a lowercase letter. With this notation,  $x$  is a realization of the random variable  $X$ .  $(X)_i$  denotes the  $i$ th element of the random variable  $X$ . These variables are multidimensional  $x \in \mathbb{R}^N$  where  $N$  is the number of pixels.  $W_x$  is a random variable associated to the wavelet transform of  $x$  and we denote  $W_{x,j}, j \in \{0, \dots, J-1\}$  ( $J$  being the number of subbands) the  $j$ th subband of the random variable  $W_x$ . We have  $w_{x,j} \in \mathbb{R}^{N_j}$  where  $N_j$  is the size of the subband. Finally, we suppose that a wavelet subband  $w_{x,j}$  follows a generalized centered Gaussian distribution law of parameter  $\alpha_{w_{x,j}} > 0$  and variance  $\sigma_{w_{x,j}}^2 > 0$  [10]. A wavelet subband probability density function  $p_{w_{x,j}}$  can then be modeled as

$$p_{w_{x,j}}(w_{x,j}) = \frac{A(\alpha_{w_{x,j}})}{\sigma_{w_{x,j}}} e^{-\left|B(\alpha_{w_{x,j}}) \frac{w_{x,j}}{\sigma_{w_{x,j}}}\right|^{\alpha_{w_{x,j}}}}, \quad (1)$$

with

$$A(\alpha_{w_{x,j}}) = \frac{\alpha_{w_{x,j}} B(\alpha_{w_{x,j}})}{2\Gamma(1/\alpha_{w_{x,j}})} \quad (2)$$

$$B(\alpha_{w_{x,j}}) = \sqrt{\frac{\Gamma(3/\alpha_{w_{x,j}})}{\Gamma(1/\alpha_{w_{x,j}})}}, \quad (3)$$

and  $\Gamma$  is the usual Gamma function. The parameters  $\sigma_{w_{x,j}}^2$  and  $\alpha_{w_{x,j}}$  of the distribution law will be estimated using the kurtosis-based technique proposed in [11]. Note that the same assumption will be applied to all wavelet transforms in the chain with, of course, different distribution parameters.

As mentioned previously, we study the imaging chain shown figure 1. We consider the special case of coding techniques based on wavelet transforms [12], [13] and [14]. The coding step is then approximately decomposed in a non-redundant wavelet transform followed by a scalar subband quantizer. Note that this approximation is actually close to the coding schemes presented in the cited works.

We also consider that the denoising step is performed in the same wavelet basis than the coding. This choice may however need further explanations. Usually, an efficient wavelet transform for image denoising strongly differs from a wavelet transform suited for image coding. Image denoising techniques actually require redundant wavelet transforms to represent the characteristics of an image such as contours and oriented details while increasing the number of coefficients in image compression may be problematic [15]. Hence, a non-redundant wavelet transform used for image compression leads most of the time to poor denoising results. We are however very confident that using the same basis for both coding and denoising may provide an optimized decoding-denoising structure gathered in a single fast and low-resources algorithm. Extending the current work to complex denoising schemes such as [16] is a difficult task that will be addressed in future works.

Based on these considerations, the studied imaging chain is represented in detail figure 2. In this chain,

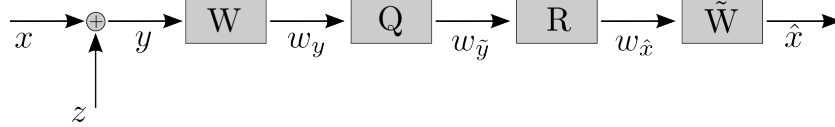


Fig. 2. Considered imaging chain

we consider the instrumental noise  $z$  to be independent, identically distributed and to follow a centered normal distribution with variance  $\sigma_z^2$ .  $\mathbf{W}$  is a wavelet transform,  $\tilde{\mathbf{W}}$  its inverse. We denote  $w_{x,j}$  and  $w_{z,j}$  to be respectively the subband  $j$  of the wavelet transform of  $x$  and  $z$ . Each quantized subband  $w_{\tilde{y},j}$  will be coded using an entropy encoder. As this operation does not introduce any degradation, it does not appear on the chain displayed figure 2.  $\mathbf{R}$  is a linear restoration algorithm which operates independently on the wavelet coefficients of each subband  $j$  of the image and writes

$$\begin{aligned} w_{\hat{x},j} = & \arg \min \|w - w_{\tilde{y},j}\|_2^2 + \lambda_j \|w\|_2^2, \\ \text{subject to } & w \in \mathbb{R}^{N_j} \end{aligned} \quad (4)$$

where  $\lambda_j > 0$  is a regularizing parameter. The restoration algorithm (4) has a closed-form solution which

writes

$$w_{\hat{x},j} = \frac{w_{\tilde{y},j}}{1 + \lambda_j}. \quad (5)$$

We are aware of the simplicity of the considered algorithm, it appears however that the linearity of the restoration algorithm  $\mathbf{R}$  is required if one wants to write the global distortion in closed-form. As mentioned previously, much work need to be addressed to consider state-of-art denoising algorithms.

The quantizer  $\mathbf{Q}$  is an infinite mid-tread scalar subband quantizer of step  $\Delta_j > 0$  and is modeled as

$$\mathbf{Q}(w_{y,j}) = \Delta_j \left\lfloor \frac{w_{y,j}}{\Delta_j} + \frac{1}{2} \right\rfloor, \quad (6)$$

where  $\lfloor \cdot \rfloor$  is the floor function which returns the greatest integer less than or equal to its argument. We now detail the basis of the proposed method to compute a closed-form expression of the global distortion. Let  $w_{b,j}$  be the coding error of the subband  $j$

$$w_{b,j} = \mathbf{Q}(w_{y,j}) - w_{y,j}. \quad (7)$$

We have

$$\begin{aligned} w_{\tilde{y},j} &= \mathbf{Q}(w_{y,j}) = w_{y,j} + w_{b,j} \\ &= w_{x,j} + w_{z,j} + w_{b,j} \\ &= w_{x,j} + w_{\epsilon,j}, \end{aligned} \quad (8)$$

where  $w_{\epsilon,j} = w_{z,j} + w_{b,j}$ . The main hypothesis of the proposed method is to consider the first-order moment of the term  $w_{\epsilon,j}$  to be independent to the one of  $w_{x,j}$ , that is

$$E[W_{\epsilon,j}W_{x,j}] = E[W_{\epsilon,j}]E[W_{x,j}], \quad (9)$$

where  $W_{\epsilon,j}$  and  $W_{x,j}$  are the random variables associated to  $w_{\epsilon,j}$  and  $w_{x,j}$ . This hypothesis is mainly based on the fact that the quantizing part of the scheme figure 2 can be seen as a non-subtractive dithering system where the Gaussian instrumental noise acts as a dithering noise.

More generally, a dithering system consists in inserting a noise with a certain probability density function prior to quantizing, to improve the decorrelation property [18]. As mentioned in [17], a non-subtractive dithering system (named non-subtractive as the dithering noise is not subtracted after quantizing) allows the moments of the global error (that is the sum of the coding error and dithering noise) to be fully decorrelated to the moments of the coding source.

It happens that a Gaussian distribution stands among the probability density functions which allow a

noise to be considered as a dithering noise. The idea here is then to take benefit of the presence of the instrumental noise by considering it as a dithering noise. With such consideration, we know that the  $m$  first-order moments of the global error are deccorelated to the  $n$  first-order moments of the quantizing source. In detail, we have for any integer  $m > 0$  and  $n > 0$  [17]

$$E [W_{\epsilon,j}^m W_{x,j}^n] = E [W_{\epsilon,j}^m] E [W_{x,j}^n] \quad (10)$$

We focus on the special case  $m = 1$  and  $n = 1$ , giving the property (9), as it is the basis of the proposed approach. Moreover, if the instrumental noise  $z$  meets the dithering noise requirements, we also have [17]

$$E [W_{\epsilon,j}] = 0, \quad (11)$$

$$E [\|W_{\epsilon,j}\|^2] = N_j \sigma_{w_{z,j}}^2 + N_j \frac{\Delta_j^2}{12}, \quad (12)$$

where  $\sigma_{w_{z,j}}$  is the standard deviation of the distribution law of the wavelet transform  $w_{z,j}$ . From [18] we know that a Gaussian noise effectively owns the properties of a dither noise if the standard deviation of its distribution law is large enough. In the present case, the condition (10) will be verified if the following statement is true

$$\sigma_{w_{z,j}} > \frac{\Delta_j}{2}. \quad (13)$$

As the standard deviation of instrumental noise is usually low in imaging systems, the condition (13) assumes that the proposed approach will be valid only for asymptotic coding rate. We will however develop our method to consider all coding rates.

### III. GLOBAL RATE-DISTORTION ANALYSIS

As mentioned in the section II, the studied imaging chain depends on two sets of parameters: The regularizing parameters  $\lambda_j$  in (5) and the quantizing steps  $\Delta_j$  in (6), for each  $j \in \{0, \dots, J-1\}$ . The global rate-distortion joint optimization problem consists in finding the optimal parameters  $\lambda_j^*$  and  $\Delta_j^*$  which minimize the global distortion  $D$  under the constraint that the coding rate  $R$  does not exceed the target rate  $R_c$ . This can be formalized as the following

$$\begin{aligned} \lambda_j^*, \Delta_j^* = & \arg \min D(\lambda_j, \Delta_j) \\ \text{subject to} & R(\lambda_j, \Delta_j) \leq R_c, \\ & \lambda_j > 0, \\ & \Delta_j > 0 \end{aligned} \quad (14)$$

Under this form, the optimization problem (14) is difficult to solve so that it is usually written under an unconstrained form. Let  $\tau > 0$  be a Lagrange multiplier. Problem (14) can then be written [19]

$$\begin{aligned} \lambda_j^*, \Delta_j^* = & \arg \min D(\lambda_j, \Delta_j) + \tau (R(\lambda_j, \Delta_j) - R_c) \quad . \\ \text{subject to} \quad & \lambda_j > 0, \\ & \Delta_j > 0, \\ & \tau > 0 \end{aligned} \quad (15)$$

To solve the global distortion joint optimization problem (15), we then need to express the global distortion  $D$  and the global coding rate  $R$  as a function of the regularizing parameters  $\lambda_j$  and the quantizing steps  $\Delta_j$ .

*Proposition 1:* If  $\sigma_{w_{x,j}}$  verifies hypothesis (13) for each  $j \in \{0, \dots, J-1\}$ , then the global distortion  $D$  of the imaging chain displayed figure 2 writes

$$D = \sum_{j=0}^{J-1} \frac{\pi_j a_j \lambda_j^2}{(1 + \lambda_j)^2} \sigma_{w_{x,j}}^2 + \frac{\pi_j a_j}{(1 + \lambda_j)^2} \sigma_{w_{z,j}}^2 + \frac{\pi_j a_j}{(1 + \lambda_j)^2} \frac{\Delta_j^2}{12}, \quad (16)$$

where

$$a_j = \frac{N_j}{N}, \quad (17)$$

is the weight of the subband  $j$  in the whole image.

*Proof:* We start from the fact that the (mean) global distortion writes

$$D = \frac{1}{N} E \left( \|X - \hat{X}\|^2 \right), \quad (18)$$

where  $\hat{X}$  is the random variable associated to the output final image  $\hat{x}$ . Thanks to the orthogonality of the wavelet subbands, the global distortion can also be formulated as

$$D = \frac{1}{N} \sum_{j=0}^{J-1} \pi_j E \left( \|W_{x,j} - W_{\hat{x},j}\|^2 \right), \quad (19)$$

where  $\pi_j$  are weighting coefficients which depend on the filters and the decimation factors used in the wavelet transform [20]. Note that these weighting coefficients are only required if one considers biorthogonal wavelet transforms such as the Cohen-Daubechies-Feauveau (CDF) 9/7 wavelet transform [21]. They are equal to 1 for an orthogonal wavelet transform.

In the case of the studied imaging chain displayed figure 2, the final image is the output of the restoration and writes

$$w_{\hat{x},j} = \mathbf{R} w_{\tilde{y},j}. \quad (20)$$



Using equations (5) and (8), the final image can be expressed as a function of the source and the global error

$$w_{\hat{x},j} = \frac{w_{x,j}}{1 + \lambda_j} + \frac{w_{\epsilon,j}}{1 + \lambda_j}. \quad (21)$$

From equations (19), (21) and using the moments decorrelation hypothesis (9), we deduce the global distortion

$$\begin{aligned} D &= \frac{1}{N} E \left( \|X - \hat{X}\|^2 \right) \\ &= \frac{1}{N} \sum_{j=0}^{J-1} \frac{\pi_j \lambda_j^2}{(1 + \lambda_j)^2} E \left( \|W_{x,j}\|^2 \right) + \frac{\pi_j}{(1 + \lambda_j)^2} E \left( \|W_{\epsilon,j}\|^2 \right). \end{aligned} \quad (22)$$

Finally, the global distortion (22) can be further developed using the results (12) to obtain the expression (16). ■

Note that the global distortion (16) requires the knowledge of the variance of each subband of the original image  $\sigma_{w_{x,j}}^2$ . This variance is generally unknown but can be deduced from the observed image if we consider an orthogonal wavelet transform. In that case, the variance of the noise in each wavelet subband  $j$  is equal to the variance of the noise in the image domain, i.e.  $\sigma_{w_{z,j}}^2 = \sigma_z^2$ , which is supposed to be known. Then,  $\sigma_{w_{x,j}}^2$  can be computed during the rate-allocation of the coder from the observed subband variance  $\sigma_{w_{y,j}}^2$  using the fact that

$$\sigma_{w_{x,j}}^2 = \sigma_{w_{y,j}}^2 - \sigma_z^2. \quad (23)$$

The second part of the problem (15) requires the expression of the global coding rate  $R$ . This rate can be expressed as the weighted sum of the rate in each subband  $R_j$

$$R = \sum_{j=0}^{J-1} a_j R_j(\Delta_j), \quad (24)$$

where  $a_j$  is given in (17). As mentioned in the hypotheses section, we assume that each quantized subband is encoded using an entropy encoder. Then, in a general non-asymptotic case, the coding rate of a subband  $j$  can be estimated by its entropy [22]

$$R_j(\Delta_j) = - \sum_{m=-\infty}^{+\infty} P_{w_{y,j}}(m, \Delta_j) \log_2 (P_{w_{y,j}}(m, \Delta_j)), \quad (25)$$

where  $P_{w_{y,j}}(m, \Delta_j)$  is the probability to get the symbol  $m$  which depends on the density probability function  $p_{w_{y,j}}$ , defined in (1), of the subband  $w_{y,j}$  and on the quantizing step  $\Delta_j$

$$P_{w_{y,j}}(m, \Delta_j) = \int_{m\Delta_j - \frac{\Delta_j}{2}}^{m\Delta_j + \frac{\Delta_j}{2}} p_{w_{y,j}}(w_{y,j}) dw_{y,j}. \quad (26)$$

As mentioned in the hypothesis section, we assume that each wavelet subband followed the generalized centered Gaussian distribution law defined in (1). The density probability function  $p_{w_{y,j}}$  is then given by:

$$p_{w_{y,j}}(w_{y,j}) = \frac{A(\alpha_{w_{y,j}})}{\sigma_{w_{y,j}}} e^{-\left|B(\alpha_{w_{y,j}}) \frac{w_{y,j}}{\sigma_{w_{y,j}}}\right|^{\alpha_{w_{y,j}}}}, \quad (27)$$

with

$$A(\alpha_{w_{y,j}}) = \frac{\alpha_{w_{y,j}} B(\alpha_{w_{y,j}})}{2\Gamma(1/\alpha_{w_{y,j}})} \quad (28)$$

$$B(\alpha_{w_{y,j}}) = \sqrt{\frac{\Gamma(3/\alpha_{w_{y,j}})}{\Gamma(1/\alpha_{w_{y,j}})}}, \quad (29)$$

and where  $\sigma_{w_{x,j}}^2$  and  $\alpha_{w_{x,j}}$  are the parameters of the distribution law, estimated using the kurtosis-based technique detailed in [11].

*Proposition 2:* The global rate-distortion optimization problem (14) can be solved by minimizing

$$\phi(\Delta_j, \lambda_j, \tau) = \sum_{j=0}^{J-1} \frac{\pi_j a_j \lambda_j^2}{(1 + \lambda_j)^2} \sigma_{w_{x,j}}^2 + \frac{\pi_j a_j}{(1 + \lambda_j)^2} \sigma_{w_{z,j}}^2 + \frac{\pi_j a_j \Delta_j^2}{12(1 + \lambda_j)^2} + \tau \left( \sum_{j=0}^{J-1} a_j R_j(\Delta_j) - R_c \right), \quad (30)$$

with respect to  $\Delta_j > 0, \lambda_j > 0$  and  $\tau > 0$ ;  $R_j(\Delta_j)$  being defined in (25).

*Proof:* This demonstration is straightforward. From equation (15), we define

$$\phi(\Delta_j, \lambda_j, \tau) = D + \tau(R - R_c), \quad (31)$$

and we substitute  $D$  and  $R$  with their respective expressions (16) and (24). ■

We detail in the next part how to minimize the criterion (30).

#### IV. GLOBAL RATE-DISTORTION OPTIMIZATION

Using proposition 2, the optimization problem (15) becomes

$$\begin{aligned} \Delta_j^*, \lambda_j^* = & \arg \min \phi(\Delta_j, \lambda_j, \tau) \quad . \\ \text{subject to} \quad & \lambda_j > 0, \\ & \Delta_j > 0, \\ & \tau > 0 \end{aligned} \quad (32)$$

The convexity analysis of the function  $\phi$  is a difficult task, such that the existence and uniqueness of solutions of problem (32) is not straightforward. We explicitly assume that a minimum of problem (32) exists, and we will show that among all the stationary points of the function  $\phi$ , only one meets the positivity constraint of the parameters. We propose a numerical algorithm to find this minimum. This algorithm is based on the resolution of the simultaneous equations obtained from the Karush-Kuhn-Tucker

(KKT) conditions [23] of problem (32).

*Proposition 3:* The KKT conditions of problem (32) admits only one solution  $(\lambda_j^*, \tau^*, \Delta_j^*)$  which verifies

$$\lambda_j^* = \frac{\sigma_{w_{z,j}}^2}{\sigma_{w_{x,j}}^2} + \frac{\Delta_j^{*2}}{12\sigma_{w_{x,j}}^2}. \quad (33)$$

$$\frac{\pi_j \Delta_j^*}{6(1 + \lambda_j^*)^2} + \tau^* \frac{\partial R_j}{\partial \Delta_j}(\Delta_j^*) = 0. \quad (34)$$

$$\sum_{j=0}^{J-1} a_j R_j(\Delta_j^*) = R_c \quad (35)$$

*Proof:* From the KKT conditions of problem (32), we get

$$\begin{cases} \frac{\partial \phi(\Delta_j^*, \lambda_j^*, \tau^*)}{\partial \Delta_j} = \frac{a_j \pi_j \Delta_j^*}{6(1 + \lambda_j^*)^2} + \tau^* a_j \frac{\partial R_j}{\partial \Delta_j}(\Delta_j^*) = 0 \\ \frac{\partial \phi(\Delta_j^*, \lambda_j^*, \tau^*)}{\partial \tau} = \sum_{j=0}^{J-1} a_j R_j(\Delta_j^*) - R_c = 0 \\ \frac{\partial \phi(\Delta_j^*, \lambda_j^*, \tau^*)}{\partial \lambda_j} = \frac{12a_j \pi_j \lambda_j^* \sigma_{w_{x,j}}^2 - 12a_j \pi_j \sigma_{w_{z,j}}^2 - a_j \pi_j \Delta_j^{*2}}{6(1 + \lambda_j^*)^3} = 0 \end{cases} \quad (36)$$

with

$$\begin{aligned} \frac{\partial R_j}{\partial \Delta_j}(\Delta_j) &= -\frac{1}{\log(2)} \sum_{m=-\infty}^{+\infty} [1 + \log(P_{w_{y,j}}(m, \Delta_j))] \times \\ &\left[ p_{w_{y,j}}\left(m\Delta_j + \frac{\Delta_j}{2}\right) \left(m + \frac{1}{2}\right) - p_{w_{y,j}}\left(m\Delta_j - \frac{\Delta_j}{2}\right) \left(m - \frac{1}{2}\right) \right]. \end{aligned} \quad (37)$$

The expressions (33), (34) and (35) of the optimal parameters directly follow from the optimality conditions (36). The uniqueness of  $\tau^*$  can be proved as follows. Using equations (33) and (34), for a given  $\tau > 0$ , we define

$$g_\tau(\Delta) = \frac{\pi_j \Delta_j}{6 \left(1 + \frac{\sigma_{w_{z,j}}^2}{\sigma_{w_{x,j}}^2} + \frac{\Delta_j^2}{12\sigma_{w_{x,j}}^2}\right)^2} + \tau \frac{\partial R_j}{\partial \Delta_j}(\Delta_j). \quad (38)$$

The coding rate  $R_j$  is a monotonically decreasing positive function with respect to  $\Delta_j$  [25],  $\Delta_j$  being positive. Its limits are zero when  $\Delta_j$  tends to infinity and infinity when  $\Delta_j$  vanishes to zero [26]. Its derivative  $\frac{\partial R_j}{\partial \Delta_j}$  is negative and monotonically increasing, whose limits are minus infinity when  $\Delta_j$  vanishes to zero and zero when  $\Delta_j$  tends to infinity [25].

We can see that the function  $g_\tau$  tends to minus infinity when  $\Delta_j$  vanishes to zero. The limit of  $g_\tau$  when  $\Delta_j$  tends to infinity is more difficult to address. When  $\Delta_j$  tends to infinity, the first term of  $g_\tau$  is positive and evolves as  $\frac{1}{\Delta_j^3}$ . The second term is negative but depending on the value of  $\tau$ , the function  $g_\tau$

may not cross zero such that the optimal quantizing step  $\Delta_j^*$  (which verifies  $g_\tau(\Delta^*) = 0$ ) may not always exist. However, this never happened in our simulations and we found out that the term  $\frac{\partial^2 R_j}{\partial \Delta_j^2}(\Delta_j)$  tends to zero quickly, when  $\Delta_j$  tends to infinity, such that  $g_\tau$  always crosses zero and therefore  $\Delta_j^*$  always exists. The uniqueness of  $\Delta_j^*$  depends on the number of times the function  $g_\tau$  crosses zero. Using the first derivative of the function  $g_\tau$ , we can show that  $g_\tau$  crosses zero only once. We have

$$g'_\tau(\Delta) = \frac{\pi_j}{6 \left(1 + \frac{\sigma_{wz,j}^2}{\sigma_{wx,j}^2} + \frac{\Delta_j^2}{12\sigma_{wx,j}^2}\right)^3} \left[ \left(1 + \frac{\sigma_{wz,j}^2}{\sigma_{wx,j}^2}\right) - \frac{\Delta_j^2}{4\sigma_{wx,j}^2} \right] + \tau \frac{\partial^2 R_j}{\partial \Delta_j^2}(\Delta_j), \quad (39)$$

To prove that  $g_\tau$  crosses zero only once, we only study the sign of the first derivative (39). From [25], we can say that  $\frac{\partial^2 R_j}{\partial \Delta_j^2}$  is positive and monotonically decreasing. From (39), we see that  $g'_\tau$  is positive when  $\Delta_j$  vanishes to zero. When  $\Delta_j$  tends to infinity, the first term of  $g'_\tau$  evolves as  $-\frac{1}{\Delta_j^4}$ . We use the same remark that the one we used for the study of  $g_\tau$  limits and we assume that  $\frac{\partial^2 R_j}{\partial \Delta_j^2}$  decreases very quickly, when  $\Delta_j$  tends to infinity, such that  $g'_\tau$  reduces to its first term. In that case, we can say that  $g'_\tau$  is negative when  $\Delta_j$  tends to infinity and, therefore, changes its sign only once.

From this result, we can conclude that the function  $g_\tau$  starts from minus infinity, crosses zero to reach its maximum and then decreases back to zero. This function crosses zero only once, implying that the optimal quantizing step  $\Delta_j^*$ , if it exists, is unique for any given  $\tau > 0$ . In this paper, we propose to compute the value of  $\Delta_j^*$  numerically using a binary search procedure. But many precautions need to be taken to be sure that we always operate on the increasing part of the function  $g_\tau$ .

From (38), we see that  $\Delta_j^*$  is function of  $\tau$ . It seems reasonable to think that the higher  $\tau$  is, the higher  $\Delta_j^*$  needs to be for the function (38) to cross zero. This implies that the optimal quantizing step  $\Delta_j^*$  can then be noted as a function of  $\tau$

$$\Delta_j^* = f(\tau), \quad (40)$$

where  $f$  is an increasing function. Consequently, from [25], we deduce that the coding rate  $R_j$  is a monotonically decreasing function with respect to  $\tau$ . Using (35) and (40), we define

$$h(\tau) = \sum_{j=0}^{J-1} a_j R_j(f(\tau)) - R_c. \quad (41)$$

Then it seems clear that the function  $h$  is a monotonically decreasing function with respect to  $\tau$  whose limits are infinity when  $\tau$  vanishes to zero and  $-R_c$  when  $\tau$  tends to infinity. Its root  $\tau^*$ , which verifies  $h(\tau^*) = 0$ , exists, is unique and can be computed using any root-finding algorithm. In our simulations, a binary search procedure will be used.

We previously showed that for any given  $\tau > 0$ , the optimal quantizing step  $\Delta_j^*$  exists and is unique. Using the uniqueness of  $\tau^*$  we can conclude that the parameters  $\tau^*$  and  $\Delta_j^*$  which verify (35) and (34) are unique. From this result and equation (33), the existence and uniqueness of the optimal regularizing parameter  $\lambda_j^*$  is straightforward to show. ■

For the sake of simplicity, each binary search algorithm will be parametrized to the same given precision  $\rho = 0.1$ . The case of the low frequency subband ( $j = J - 1$ ) will be processed differently as we do not want to degrade these coefficients. We will only use quantizing to round these coefficients to their nearest integers. Consequently, we will set

$$\Delta_{J-1}^* = 1, \quad (42)$$

$$\lambda_{J-1}^* = \frac{\sigma_{w_{z,J-1}}^2}{\sigma_{w_{x,J-1}}^2} + \frac{1}{12\sigma_{w_{x,J-1}}^2}. \quad (43)$$

Finally, the overall joint optimization procedure for solving problem (14) is given in the algorithm 1. Note that the binary search sub-procedures are not detailed in this process. The algorithm 1 intends to be quite general and we let the choice of the root-finding algorithms to the user.

## V. RESULTS

We simulate the joint optimization algorithm 1 on the well-known test images *Lena*, *Barbara*, *Pirate* and on the high-dynamic range remote sensing image displayed figure 3. For this simulation, we set the wavelet transform  $\mathbf{W}$  to be a three levels CDF 9/7 wavelet transform [21] and  $\mathbf{R}$  is given by (4). Each test image has been noised with an additive white Gaussian noise with a standard deviation  $\sigma_z$  equal to 15. As the efficiency of the proposed estimation depends on the standard deviation of this noise (see equation (13)), we simulate two more cases for the *Barbara* image:  $\sigma_z = 5$  and  $\sigma_z = 25$ .

For each target rate, we simulate the imaging chain 2 with the usual disjoint optimization technique, which consists in selecting the quantizing steps and the regularizing parameters such that the coding and the restoration errors are independently minimized. The coding error minimization has been achieved using the rate-distortion allocation based model proposed in [24]. As for the restoration error, it has been minimized using an exhaustive search of the optimal regularizing parameters. Once the final image has been reconstructed using these parameters, we numerically compute the global distortion

$$D = \frac{1}{N} \|x - \hat{x}\|^2, \quad (44)$$

where  $x$  is the clean test image (assumed to be known in our numerical experiments) and  $\hat{x}$  is the final image. The distortion (44) is the true distortion and will be referred as the ground truth in our simulations.

---

**Algorithm 1** Global rate-distortion joint optimization algorithm

---

```

Set  $\tau = 1$ .
Set  $\rho = 0.1$ .
while  $\left| \sum_{j=0}^{J-1} a_j R_j - R_c \right| > \rho$  do
  for  $j$  from 0 to  $J - 2$  do
    Set  $\Delta_j = 1$ .
    Compute the value of the regularizing parameter  $\lambda_j$  from (33).
    while  $\left| \frac{\pi_j \Delta_j}{6(1+\lambda_j)^2} + \tau \frac{\partial R_j}{\partial \Delta_j}(\Delta_j) \right| > \rho$  do
      Increase the value of  $\Delta_j$ .
      Compute the value of the regularizing parameter  $\lambda_j$  from (33).
    end while
  end for
  Compute the regularizing parameter  $\lambda_{J-1}$  from (42).
  Compute the quantizing step  $\Delta_{J-1}$  from (42).
  if  $\left| \sum_{j=0}^{J-1} a_j R_j - R_c \right| > \rho$  then
    Increase the value of  $\tau$ .
  end if
end while
Output the optimal regularizing parameters  $\lambda_j^*$ .
Output the optimal quantizing steps  $\Delta_j^*$ .

```

---

The estimation model (16) of the global distortion that we proposed has then been computed with the values of parameters obtained for the ground truth. This allows to verify that the estimation (16) of the global distortion is close to the ground truth (44), implying the validity of the proposed method. And finally, we use the proposed joint optimization algorithm 1 to compute the optimal parameters, that we inserted into the estimation model (16) to compute the minimal distortion.

The resulting rate-distortion curves are given figures 4 to 8. We see that the validity of the proposed estimation, as expected by the hypothesis (13), is not always verified and depends on the target coding rate. More precisely, the proposed estimation approximates well the true distortion for medium to high coding rates but does not give satisfying results for low coding rates. This can be explained by the



(a)



(b)



(c)



(d)

Fig. 3. Test images: (a) is *Lena* ( $256 \times 256$  pixels), (b) is *Barbara* ( $512 \times 512$  pixels), (c) is *Pirate* ( $1024 \times 1024$  pixels) and (d) is a high-dynamic range remote sensing image (12 bits) of Cannes harbour ( $1024 \times 1024$  pixels).

fact that for low coding rates, the condition (13) is not respected anymore and that the moments of the global error cannot consequently be considered decorrelated to the moments of the source. As mentioned previously, we performed several simulations on the *Barbara* image with different standard deviations of the noise such that the condition (13) can be verified for different ranges of coding rate. When the standard deviation is low (figure 5), we see that the proposed estimation is performant if the coding rate is around 2.5 bits/pixel and more. However for this high coding rate, the coding step is almost lossless such that the global optimization problem is reduced to the optimization of the restoration only. Therefore, the joint and the disjoint optimization techniques become the same and give then similar results.

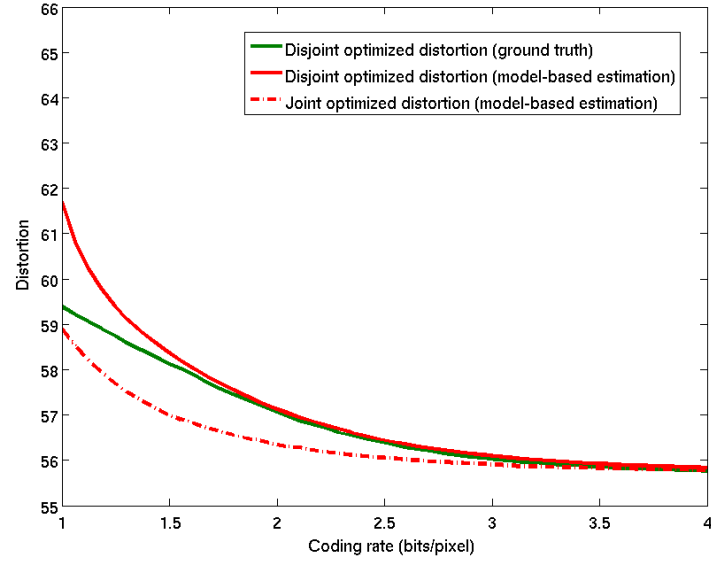


Fig. 4. Comparison of the disjoint optimized distortion (ground truth and model-based estimation) to the joint optimized distortion (model-based estimation) on *Lena*,  $\sigma_z = 15$ .

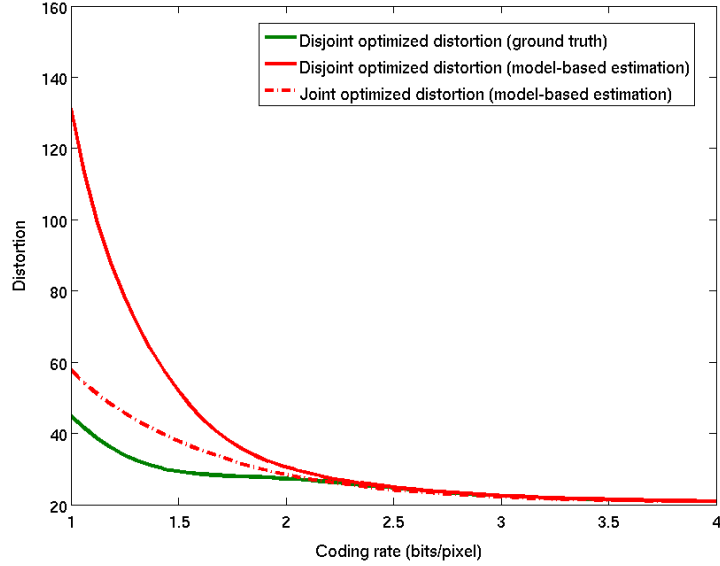


Fig. 5. Comparison of the disjoint optimized distortion (ground truth and model-based estimation) to the joint optimized distortion (model-based estimation) on *Barbara*,  $\sigma_z = 5$ .



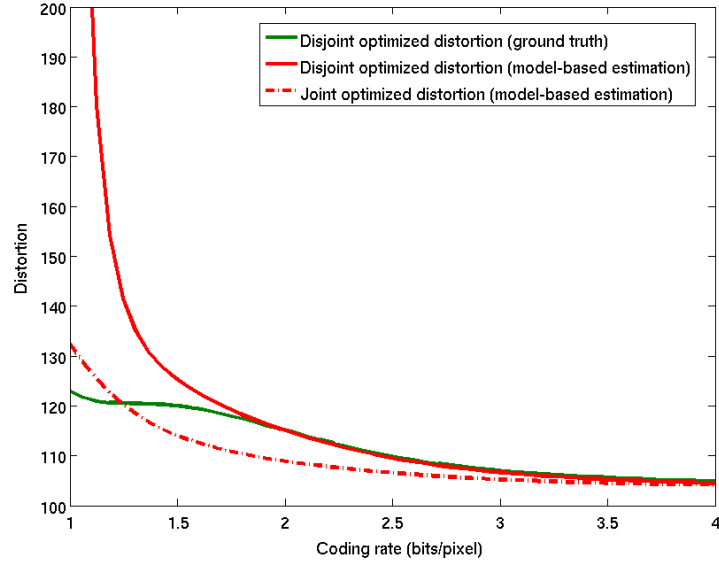


Fig. 6. Comparison of the disjoint optimized distortion (ground truth and model-based estimation) to the joint optimized distortion (model-based estimation) on *Barbara*,  $\sigma_z = 15$ .

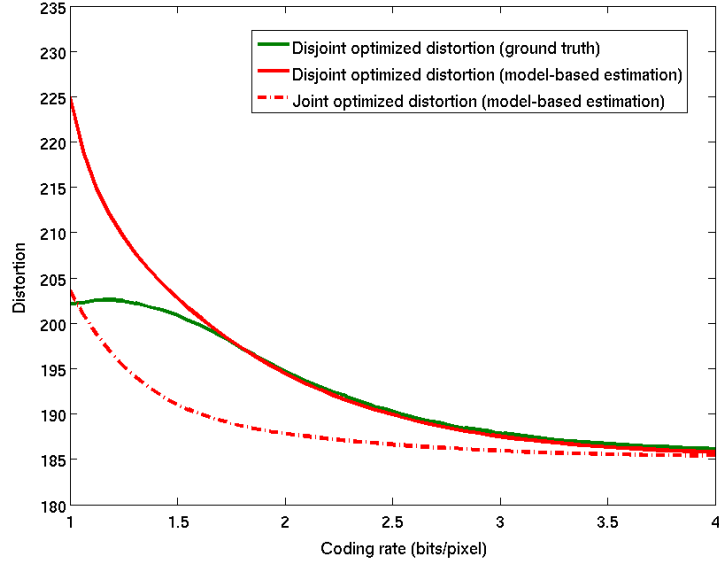


Fig. 7. Comparison of the disjoint optimized distortion (ground truth and model-based estimation) to the joint optimized distortion (model-based estimation) on *Barbara*,  $\sigma_z = 25$ .

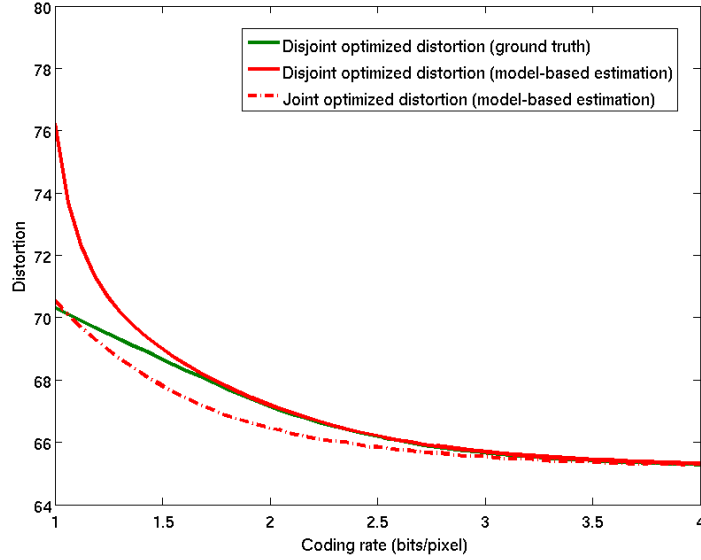


Fig. 8. Comparison of the disjoint optimized distortion (ground truth and model-based estimation) to the joint optimized distortion (model-based estimation) on *Pirate*,  $\sigma_z = 15$ .

As shown by the figures 5, 6 and 7, the range of validity of the proposed estimation increases as the standard deviation increases. For a high standard deviation (figure 7), we can verify that the proposed estimation is valid for lower coding rates (around 1.8 bits/pixel and more). In that case, the joint optimization displays significant improvement in comparison to the disjoint optimization. It allows for example to reach the same global error than the disjoint optimized technique but for a lower coding rate. On the *Barbara* image and for  $\sigma_z = 15$  (figure 6), the joint optimization technique reaches at 1.42 bits/pixel the same distortion than the one obtained at 2.04 bits/pixels for the disjoint optimization technique, saving therefore almost 30% of the bit budget. The benefit in term of compression performances of the joint optimization technique appears then to be very significant.

Visual results for the target rate of 2.5 bits/pixel are given figures 9 to 12 for the high-dynamic range remote sensing image. We do not focus on the quality of the reconstructed images regarding to the reference one as the considered chain is excessively simple. Clearly, the presence of artifacts on the reconstructed image is due to the simple hypothesis that we made on the restoration algorithm (4). On the contrary, we are more concerned on the improvement of the image quality of the joint optimized

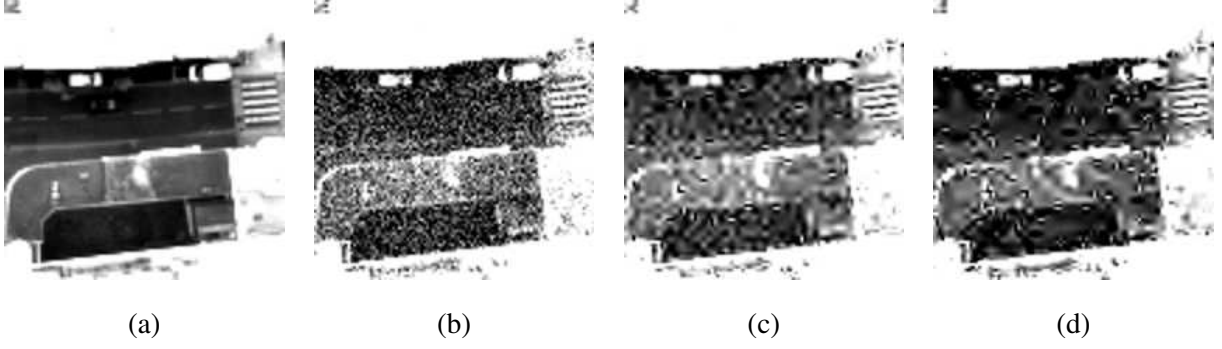


Fig. 9. Visual comparison of reconstruction results. (a) is the reference image, (b) is the observed image, (c) is the image reconstructed with the parameters obtained by the minimizing the measured distortion and (d) is the image reconstructed with the parameters obtained by the model-based optimization algorithm 1. The coding rate is 2.5 bits/pixel. The image range has been extended to point up the image reconstruction artifacts.

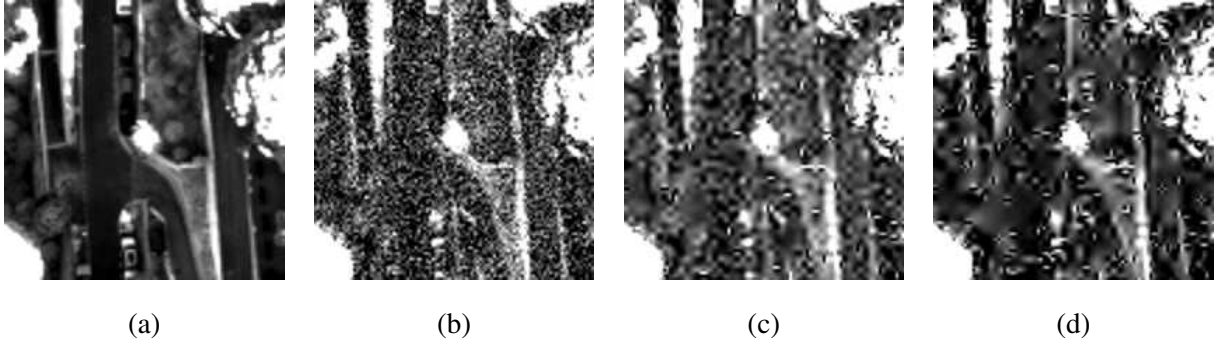


Fig. 10. Visual comparison of reconstruction results. (a) is the reference image, (b) is the observed image, (c) is the image reconstructed with the parameters obtained by the minimizing the measured distortion and (d) is the image reconstructed with the parameters obtained by the model-based optimization algorithm 1. The coding rate is 2.5 bits/pixel. The image range has been extended to point up the image reconstruction artifacts.

chain with respect to the disjoint optimized one. We can see that the global joint optimization of the chain always leads to a reconstructed image which contains less blurry edges or ringing artifacts. This is particularly visible on the edges of the buildings figures 9 and 11. As mentioned in the introduction of this paper, the obtained results clearly point that optimizing coding and denoising separately is suboptimal. One needs instead to address the problem of imaging chain design in its globality; the proposed method and the obtained results are encouraging in this sense. A lot of work is however required to extend the proposed method to lower coding rates and to more complex denoising schemes.

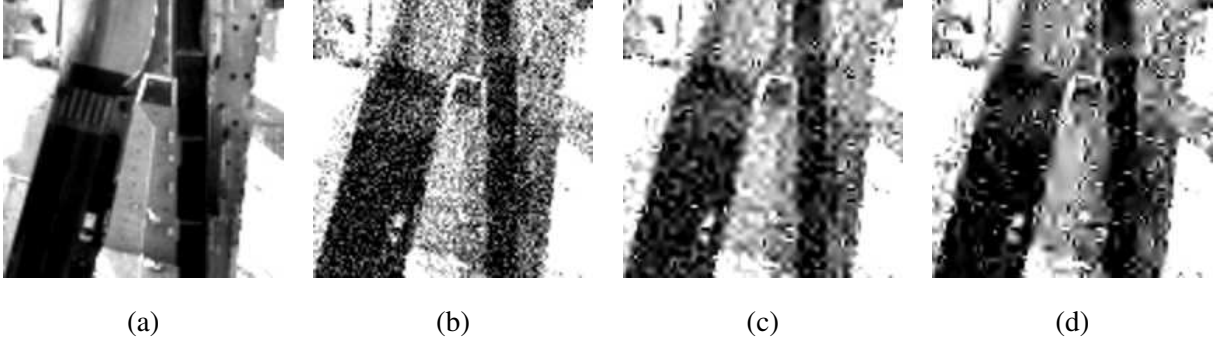


Fig. 11. Visual comparison of reconstruction results. (a) is the reference image, (b) is the observed image, (c) is the image reconstructed with the parameters obtained by the minimizing the measured distortion and (d) is the image reconstructed with the parameters obtained by the model-based optimization algorithm 1. The coding rate is 2.5 bits/pixel. The image range has been extended to point up the image reconstruction artifacts.

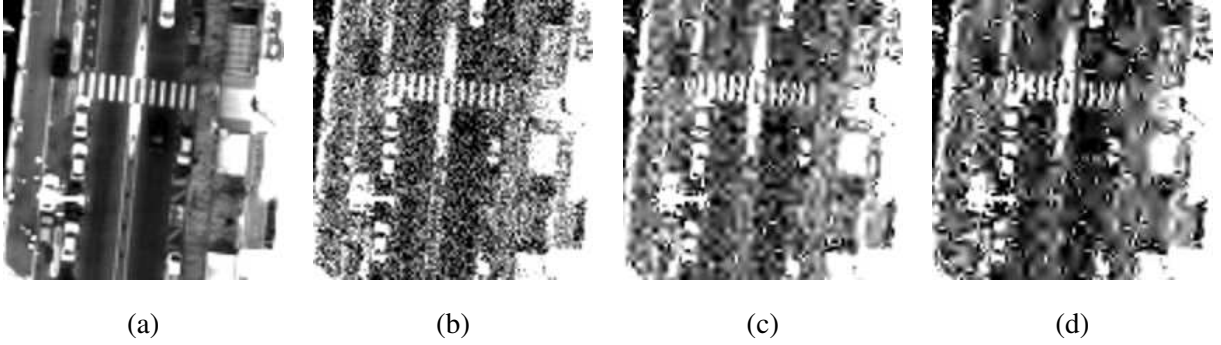


Fig. 12. Visual comparison of reconstruction results. (a) is the reference image, (b) is the observed image, (c) is the image reconstructed with the parameters obtained by the minimizing the measured distortion and (d) is the image reconstructed with the parameters obtained by the model-based optimization algorithm 1. The coding rate is 2.5 bits/pixel. The image range has been extended to point up the image reconstruction artifacts.

## VI. CONCLUSIONS

In this paper we considered the problem of joint noisy source coding/denoising. Most of the time, the coding and the denoising parameters are selected independently such that the coding and the restoration error are respectively minimized. This parameters selection technique leads however to a suboptimal distortion. It appears then crucial to address the problem of joint coding/denoising in its globality. We proposed here a technique to modelize the global distortion and we presented an algorithm to get the optimal coding and denoising parameters. We simulated this joint optimization technique on classical test

images and on a high-dynamic range remote sensing image. We concluded that our joint coding/denoising optimization approach can either allows to reach the same quality at lower rates or to improve the quality of the reconstructed final image for the same rates, in comparison to the image obtained using the classical disjoint optimization technique. Further works will be focussed on the extension of the proposed model to lower coding rates and to advanced denoising schemes.

## REFERENCES

- [1] S.-C.B. Lo, B. Krasner, S.K. Mun. Noise impact on error-free image compression. *IEEE Transactions on Medical Imaging*, 9(2):202–206, 1990.
- [2] R. Dobrushin, B. Tsybakov. Information transmission with additional noise. *IEEE Transactions on Information Theory*, 8(5):293–304, 1962.
- [3] E. Ayanoglu. On optimal quantization of noisy sources. *IEEE Transactions on Information Theory*, 36(6):1450–1452, 1990.
- [4] Y. Ephraim, R.M. Gray. A unified approach for encoding clean and noisy sources by means of waveform and autoregressive model vector quantization. *IEEE Transactions on Information Theory*, 34(4):826–834, 1988.
- [5] D. Sakrison. Source encoding in the presence of random disturbance. *IEEE Transactions on Information Theory*, 14(1):165–167, 1968.
- [6] J. Wolf, J. Ziv. Transmission of noisy information to a noisy receiver with minimum distortion. *IEEE Transactions on Information Theory*, 16(4):406–411, 1970.
- [7] D. Rebollo-Monedero, S. Rane, B. Girod. Wyner-Ziv quantization and transform coding of noisy sources at high rates. *Asilomar Conference on Signals, Systems and Computers*, 2(1):2084–2088, 2004.
- [8] T.R. Fischer, J.D. Gibson, B. Koo. Estimation and noisy source coding. *IEEE Transactions on Acoustics, Speech and Signal Processing*, 38(1):23–34, 1990.
- [9] O.K. Al-Shaykh, R.M. Mersereau. Lossy compression of noisy images. *IEEE Transactions on Image Processing*, 7(12):1641–1652, 1998.
- [10] M. Antonini, M. Barlaud, P. Mathieu, P. and I. Daubechies. Image coding using wavelet transform. *IEEE Transactions on Image Processing*, 1(2):205–220, 1992.
- [11] J.H. Kasner, M.W. Marcellin, B.R. Hunt. Universal trellis coded quantization. *IEEE Transactions on Image Processing*, 8(12):1677–1687, 1999.
- [12] J.M. Shapiro. Embedded image coding using zerotrees of wavelet coefficients. *IEEE Transactions on Signal Processing*, 41(12):3445–3462, 1993.
- [13] A. Said and W.A. Pearlman. A new, fast, and efficient image codec based on set partitioning in hierarchical trees. *IEEE Transactions on Circuits and Systems for Video Technology*, 6(3):243–250, 1996.
- [14] D. Taubman. High performance scalable image compression with EBCOT. *IEEE Transactions on Image Processing*, 9(7):1158–1170, 2000.
- [15] V. Chappelier and C. Guillemot. Oriented Wavelet Transform for Image Compression and Denoising. *IEEE Transactions on Image Processing*, 15(10):2892–2903, 2006.
- [16] D.L. Donoho. De-noising by soft-thresholding. *IEEE Transactions on Information Theory*, 41(3):613–627, 1995.
- [17] R.A. Wannamaker, S.P. Lipshitz, J. Vanderkooy, J.N. Wright. A theory of nonsubtractive dither. *IEEE Transactions on Signal Processing*, 48(2):499–516, 2000.

- [18] J. Vanderkooy, S.P. Lipshitz. Dither in Digital Audio. *Journal of the Audio Engineering Society*, 35(12):966–975, 1987.
- [19] H. Everett. Generalized Lagrange Multiplier Method for Solving Problems of Optimum Allocation of Resources. *Operations Research*, 11(3):399–417, 1963.
- [20] B. Usevitch. Optimal bit allocation for biorthogonal wavelet coding. *Data Compression Conference*, 387–395, 1996.
- [21] A. Cohen, I. Daubechies, J.-C. Feauveau. Biorthogonal bases of compactly supported wavelets. *Communications on Pure and Applied Mathematics*, 45(5):485–560, 1992.
- [22] C.E. Shannon. A Mathematical Theory of Communication. *Bell System Technical Journal*, 27(3):379–423, 1948.
- [23] H.W. Kuhn, A.W. Tucker. Nonlinear programming. *Berkeley Symposium on Mathematical Statistics and Probability*, 481–492, 1951.
- [24] C. Parisot, M. Antonini, M. Barlaud, S. Tramini, C. Latry and C. Lambert-Nebout. Optimization of the Joint Coding/decoding Structure. *IEEE International Conference on Image Processing*, 2001.
- [25] C.E. Shannon. Coding theorems for a discrete source with a fidelity criterion. *IRE International Convention Record*, 7:142–163, 1959.
- [26] H. Gish, J. Pierce. Asymptotically efficient quantizing. *IEEE Transactions on Information Theory*, 14(5):676–683, 1968.